

Received February 6, 2020, accepted February 28, 2020, date of publication March 4, 2020, date of current version April 7, 2020.

Digital Object Identifier 10.1109/ACCESS.2020.2978245

An Improved Unscented Particle Filter Method for Remaining Useful Life Prognostic of Lithium-ion Batteries With Li(NiMnCo)O₂ Cathode With Capacity Diving

XINWEI CONG^{ID}¹, (Student Member, IEEE), CAIPING ZHANG^{ID}¹, (Senior Member, IEEE), JIUCHUN JIANG^{ID}^{2,3}, (Senior Member, IEEE), WEIGE ZHANG^{ID}¹, YAN JIANG^{ID}^{4,5}, AND XINYU JIA¹

¹National Active Distribution Network Technology Research Center (NANTEC), Beijing Jiaotong University, Beijing 100044, China

²Shenzhen Precise Testing Technology Company Ltd., Shenzhen 518100, China

³School of Electrical and Electronic Engineering, Hubei University of Technology, Hubei 432200, China

⁴Sunwoda Electronic Company Ltd., Shenzhen 518108, China

⁵School of Electric Power, South China University of Technology, Guangzhou 510640, China

Corresponding authors: Caiping Zhang (zhangcaiping@bjtu.edu.cn) and Jiuchun Jiang (jcjiang@bjtu.edu.cn)

This work was supported in part by the National Key Research and Development Program of China under Grant 2018YFB0905304, and in part by the National Natural Science Foundation of China under Grant U1664255, Grant 61633015, and Grant 51977007.

ABSTRACT An improved method for the remaining useful life (RUL) prognostic of Lithium-ion batteries with Li(NiMnCo)O₂ cathode using improved unscented particle filter (UPF) is proposed with respect to capacity diving in later capacity degradation curve. Key points of this paper are: (1) An appropriate empirical model for the situation as the most contributive work, is put forward as an alternative to the widely used UPF models, and the prediction performance is respectively verified by least square fitting and the improved UPF; (2) Systematic noise in Gamma distribution is attempted in state space equations of the proposed method, so as to avoid potential shape shifting of the prediction curve after sampling the particles with Gaussian noise, for model parameters could get zero-crossed; (3) With training data preprocessed considering the capacity recovery phenomenon concisely, the residual error and root mean square error of fitting could get further reduced, as a supplement to traditional treatments like smoothing, thus relieving the sensitivity of data-driven methods to data by enhancing quality. Validations are implemented by applying the proposed method to the battery data by conducting cycle aging tests under different working conditions, where improved approximation and prediction performance can be obtained.

INDEX TERMS Lithium-ion battery, remaining useful life, state of health, unscented particle filter, capacity diving phenomenon.

I. INTRODUCTION

Lithium-ion batteries are widely applied for excellent performance in various aspects, and the safety and reliability problems of Lithium-ion batteries have aroused a lot of attention [1]. The prediction of the remaining useful life (RUL) of Lithium-ion batteries plays an important role in state of health (SOH) estimation, providing evidence for decision

The associate editor coordinating the review of this manuscript and approving it for publication was Ziang Zhang^{ID}.

makers to avoid malfunctions thus running the system appropriately and reducing loss [2].

A. REVIEW OF THE APPROACHES

As reviewed in [1], two main concepts concerning the prediction of the RUL of Lithium-ion batteries are illustrated. Employing the observation in a past period of cycles, the physics of failure methods as the first concept critically relies on absolute accuracy of the life time model and measurement [3], [4], and no recalibration considering present SOH features can be seen. Besides, on account of

the incompleteness of precise description of sophisticated electrochemical behavior, material properties, constructions, and fading mechanism of Lithium-ion batteries [4], the other concept known as data-driven methods is preferable by analyzing the characteristics featuring SOH, like capacity and impedance, so as to track the degradation until they reach the threshold value defined as the end of life (EOL) point.

Under the second circumstance of adopting data-driven methods, frameworks of great simplicity and efficient implementation are utilized for aging predictions of Lithium-ion batteries. There are many completed case studies in which good predicting performance can be seen by typically using fitting [6], [20], machine learning (Neural Network (NN) [7], Supporter Vector Machine (SVM) [8], and Relevance Vector Machine (RVM) [9]), signal processing [10], [11], and statistical regression based on probabilistic methods (Auto Regressive Model Average [10], [12], Grey Model (GM) [13], [14], and process regressions [15]–[17], [27]) etc. Explicitly, researchers are provided with informative results in an analytical probabilistic form when demonstrating the problems with uncertainty and nonlinearity by probabilistic analysis methods, especially methods based on Bayesian theories. So the difficulties in expressing accurate predictions are resolved, for the outcome in the form of expectations and confidence intervals promisingly assists in making wise decisions. And it has become an inevitable trend for researchers to combine the abovementioned methods to make various algorithm improvements.

The accuracy of extended Kalman filter (EKF) and unscented Kalman filter (UKF), and sequential Bayesian Monte Carlo methods, like several particle filters, has been theoretically evaluated by the Kullback–Leibler and χ^2 information measure respectively [18]. Corresponding to the RUL prediction with non-linear capacity degradation, one of the sequential Monte Carlo methods combining UKF and particle filter (PF)—unscented particle filter (UPF) is outstanding for the relatively highest approximation at the expense of computational cost.

The main idea of PF can be generally thought as using random particles and their weights to approximate the posterior probability distributions of the system states, which is realized through the procedure of sequential importance sampling, suffering possible problems as sample degeneracy and particle impoverishment [29], [31]. Saha *et al.* [12] revealed that, PF has better accuracy than ARIMA, EKF, RVM, and SVM by a comparative study of the algorithm performance for RUL predictions. Besides, Miao *et al.* [19] made several representative works to verify the practical performance of UPF in RUL prediction, compared with PF in a lot of case studies, with the vast majority of the results showing the optimal choice is UPF among this category. Except for the UKF used as the importance function in PF to make up for the demerits, others like spherical cubature particle filter has also been proposed to provide an importance function for particle filter for battery prognostics by Wang *et al.* [31], showing

better performance than PF in RUL prediction, of which determination of the sigma points is similar to UPF.

Since UPF implementation makes sure that, parameters in the model are only updated up to the last one moment, good robustness is theoretically guaranteed in the regression process. As a consequence, a couple of initial training data of unstable quality caused by the activation effect of the batteries will exert promptly decreasing influence with the process of subsequent UPF iteration. That is to say, now that training data are divided into different sections with variant systematic noise in RUL prediction when capacity diving occurs, training information with poor quality in very early periods could be gradually vanishing in later loops of UPF, leading to superior performance of local iteration [19], and with further considering the computational cost and available training information quantity, UPF is chosen rather than artificial intelligence methods in the paper to deal with the problem.

A dynamic state space system model used in UPF usually consists of a state transition model and a measurement model. The state transition function plays a critical role in particle sampling, and the measurement equation, regularly known as the empirical model with a noise term, is required to be sufficiently precise in actual observation, and concise thus not over-fitting.

With respect to the measurement model part, intuitively speaking, traditional combinations of simplex exponential function terms and power function terms in the measurement equation used in existing study [5], [8], [23], [24] are too smooth to describe rapidly decreasing tendency in later capacity degradation curve. There are quantities of cases [20] in which, very long flat capacity curve of early training data with slow degradation provides the identification of model parameters representing later plunging capacity degradation with very insufficient training information, thus making difficulties in determining how much training information is necessarily used at least. Besides, an immense quantity of training information is required using the method in [20]. Since these prediction works using only capacity information are conducted absent of the consideration of the training data with capacity diving, there is a need to verify the performance of various models to find a better empirical model as a specific measurement equation suitable for the RUL prediction of capacity diving problem.

As for the state transition model part, the procedure of sampling, as well as resampling, is of great significance in UPF algorithm study [22], of which the state noise usually is in the form of Gaussian distribution for each model parameter dimension. However, assuming distinct plunging tendency appears in the later capacity degradation curve, even if UPF could follow the extent of changing tendency by varying the covariance matrix in the iteration process, the systematic noise could be constantly changing in an unsatisfying response speed around and after the inflection point. As a result, poor convergence speed of the algorithm demands abundant training information, which could lead to

very frustrating prediction performance. Meanwhile, a wide value range to determine among noise parameters sacrifices the robustness of the stability and validity of the model for rapid convergence of the algorithm, because irrational shape shifting could occur in subsequent prediction for parameter zero-crossing takes place among the parameters during particle sampling.

Moreover, data quality enhancement is of vital significance in that data-driven methods are sensitive to data quality to a large extent. In addition to common preprocessing strategies, the capacity self-recharge brought by performance tests during aging tests should be taken into account. After quantities of work done to data preprocessing for a long time, recently in 2019, Pang *et al.* [25] made the problem resolved effectively using a combination of wavelet decomposition and artificial intelligence methods, and made RUL predictions to compare the performance of three proposed models showing the WDT-NARNN method among them to be reasonable and suitable. Besides, Zhao *et al.* [26] verified the degradation process by applying RVM and GM methods to the proposed capacity regeneration and normal degradation model, developing a hybrid method for RUL estimation, and Xu *et al.* [30] adopted Wiener process methods to make a successful RUL prediction, with the consideration of capacity relaxation effects. The essential target of establishing a capacity recovery function is to demonstrate the impacts brought by the capacity recovery phenomenon after battery performance tests on the empirical model, and it is inevitable that training data preprocessed without considering the factor of capacity recovery phenomenon will bring unsupported information to actual measurement equation of the algorithm, leading to reduction in the model precision and stability of the regression process. Since there are many cases in which, when to conduct experimentally designed performance tests is already known, therefore simplifications could be made by merely verifying several fading characteristics based on current studies.

B. CONTRIBUTION OF THE PAPER

1) DATA QUALITY ENHANCEMENT

Brief steps are stated as follows.

Firstly, obvious outliers are recognized and eliminated by statistical methods. Next, a further simplified capacity recovery function $T(x)$ is developed, of which the identification of parameter values becomes the major contribution of the paper to the part of data quality enhancement. Then Savitzky-Golay filtering is implemented to measurement noise smoothing, because of its better processing performance compared to the widely used moving average filter [2].

2) IMPROVEMENT OF THE STATE SPACE EQUATIONS

The contributions of the paper to the state space equations of the model are divided into 2 following parts:

- (1) A modified empirical capacity fading model is developed in the paper for a specific description of capacity

diving, with comparison cases made to verify RUL prediction performance in both the early capacity curve and the whole curve;

- (2) Chances are that some terms in the measurement equation represents the early characteristics, and other terms have close contact with the later sharp decline. So considering the shape factor of the curve derived from measurement equations, the state transition equations are improved by sectioned treatment of sampling using inflection point checking technique and noises in Gamma distribution.

II. IMPROVEMENTS

A. SIMPLIFIED CAPACITY RECOVERY FUNCTION

By merely verifying a couple of fading characteristics as in [26], a further simplified $T(x)$ for preprocessing data efficiently is developed as (1) to demonstrate the relationship between the measurement equation and the observed capacity data with experimental designed performance tests information already known,

$$\begin{cases} H(x) = C(x) - T(x) \\ T(x) = \sum^n \rho_n e^{-\frac{1}{\tau_n}(x-t_n)} \cdot \mathbf{1}(x-t_n) + Q_{cal} \end{cases} \quad (1)$$

where $H(x)$ denotes the empirical model as a main part of the measurement function in the methods, $C(x)$ denotes experimental capacity degradation curve, n denotes the total number of times of performance tests, ρ_n denotes the peak value of the n th performance test, τ_n denotes the time constant of the n th performance test, t_n denotes the moment of the n th performance test known by designed experimental procedure, and $\mathbf{1}(x-t_n)$ denotes the unit step response function with the jump taking place at moment t_n . Considering aging tests in lab experimental conditions, the capacity recovery of calendar loss term Q_{cal} could be negligible due to short cyclic interval periods. The parameters could be obtained by the procedure in Table 1.

TABLE 1. Acquirement of the parameters of $T(x)$.

Parameter	Approaches
t_n	By the practical experimental procedure
ρ_n	By differential value after the performance test, $C(t_n) - C(t_n - 1)$
τ_n	τ_n defined by when the response value is reduced to e^{-1} times of ρ_n
	$3\tau_n$ determined by when the slope of the linkage of $t_n - 1$ and current point is almost equal to the slope of tangent of the capacity degradation curve

Residual error (RSE) and root mean square error (RMSE) of fitting training data using empirical models are considerably reduced, which is mainly attributed to well-illustrated impacts on the capacity degradation curve brought by performance tests during cyclic aging tests.

B. STATE SPACE EQUATIONS

1) THE MEASUREMENT EQUATION

For the empirical model part, Bayesian Information Criterion (BIC) is commonly utilized as a general indicator in model performance evaluation, with a smaller BIC value indicating the better balanced performance in approximation and complexity of the model shown as (2),

$$BIC = K \ln(n) - 2 \ln(f(y | \theta_k)) \quad (2)$$

where $f(y | \theta_k)$ denotes the maximum likelihood function indicating the accuracy, n denotes the quantity of the data records, and K denotes the quantity of the parameter of the polynomial fitting indicating the complexity. In order to obtain a model with small BIC value, it is preferable that K value is small implying the model not over-fit. Exponential function terms are splendid for their concise, smoothness and diversity of shape, and the simplex exponential function is Taylor expanded in (3),

$$e^x = 1 + \frac{x^1}{1!} + \frac{x^2}{2!} + \cdots = \sum_{n=0}^{\infty} \frac{x^n}{n!} \quad (3)$$

Generally a couple of expanded polynomial terms as the neighborhood of the Taylor expansion approximation are of practical use, for which the number of exponential-shaped terms involved in the model to discuss in the paper is not more than 2, because severe punishment of BIC will take place if K is empirically larger than 7.

The double exponential function has been put forward as the most widely used model by far [5] shown as (4),

$$H(x) = a_1 e^{b_1 x} + a_2 e^{b_2 x}, \quad x \in N^+ \quad (4)$$

and a single exponential function in [23] is shown as (5),

$$H(x) = \beta_1 + \beta_2 e^{\frac{\beta_3}{x}}, \quad x \in N^+ \quad (5)$$

despite BIC of an single exponential model could take advantage of reduced quantity of parameters, the observation error is enormously large to describe the capacity degradation curve validated in the abovementioned work. As for polynomial function terms, a model with such a term to describe the decline empirically has been put forward in [8],

$$H(x) = a_1 e^{b_1 x} + a_2 x^{b_2}, \quad x \in N^+ \quad (6)$$

where a large integer is selected as the value of b_2 , as fast recession later in the data is judged by experience, otherwise a little integer is chosen.

Models with other complicated forms of terms [24], like the double Gaussian shown as (7),

$$H(x) = a_1 e^{\frac{(x-\mu_1)^2}{\gamma_1}} + a_2 e^{\frac{(x-\mu_2)^2}{\gamma_2}}, \quad x \in N^+ \quad (7)$$

the exponential combined with the multi-polymal,

$$H(x) = a_1 e^{b_1 x} + \sum_{i=2}^n a_i x^{b_i}, \quad x \in N^+, n \geq 3 \quad (8)$$

and etc. are excluded from the discussion because of either large K value in BIC or particular requirements of scarce applied conditions.

Combined with part of the abovementioned models, and inspired by the piecewise based attempts, the empirical model used in the measurement equation is proposed as (9),

$$H(x) = C(x) - T(x) = ae^{\frac{b}{x}} + ce^{dx}, \quad x \in N^+ \quad (9)$$

where the incoming moment and sharpness degree of the capacity diving in the later curve are indicated by later stage term $ae^{\frac{b}{x}}$, and initial capacity is indicated by c with the extent of early degradation indicated by d in the early stage term ce^{dx} .

2) THE STATE TRANSITION FUNCTION

The state transition function used in existing study is regularly in the form as (10),

$$x_{i,k} = F \cdot x_{i,k-1} + w_i, \quad w_i \sim N_i(0, \sigma_i^2), \quad i = 1, 2, \dots, n \quad (10)$$

where F is the state transfer matrix, normally expressed in a diagonal form with constants like 1, and w_i is the systematic noise in Gaussian distribution N_i . Generally, as the selected methods are applied in Gaussian noise conditions, the iteration of the state transition function is composed of the parameter value of the last moment and a 0-mean Gaussian noise term for each parameter dimension, and when particles are sampled, σ_i^2 of relevant terms can be updated by corresponding UKF parts after initialization.

Early data of the training data set reflects the dominant effect caused by the early stage term ce^{dx} ($c > 0, d < 0$) in the measurement equation, and little information related to the later period term $ae^{\frac{b}{x}}$ ($a < 0, b < 0$) is referred to, which is attributed to the different sensitivity of parameters at different moments. In [29], PF methods are adopted in GA algorithm in the process of resampling, thus influencing the passing of the parameters between different moments. Therefore, it is available that time-varying modulation is applied to the covariance matrix of state functions, with the form of state noise distribution taken into account.

Choosing Gaussian noise is appropriate to satisfy sampling requirement of the UKF algorithm, and relieving the non-linearity but the variances in different dimensions of the equation are still relatively independent in (10), which is supposed to be in the form of covariance matrix. Furthermore, shape shifting of the prediction curve could occur as it is inevitable for particle sampling by Gaussian noise to meet zero crossing conditions—the possible value range of some of the parameters becomes very wide, generating large distribution variances to sample the particles with insufficient training information, of which the distribution covers the zero point in early iterations. Consequently, the iterative performance of the measurement equation like double exponential function is severely affected with questionable correctness, so in this case sampling parameters have to be set small enough to limit the diversity and the range of particles. Besides, when the terms representing different stages are determined, empirical evidence and 95% fitting intervals of

training data could help to judge the sampling parameters. Finally, three basic characteristics of Gamma distribution $Ga(\alpha, \beta)$ ($\alpha, \beta > 0$) make it appropriately applied as a solution to the situation,

$$X \sim Ga(\alpha, \beta) (\alpha, \beta > 0) \\ s.t. f(X) = \frac{\beta^\alpha}{\Gamma(\alpha)} X^{\alpha-1} e^{-\beta X}, \quad X > 0 \quad (11)$$

where $f(X)$ is the probability distribution function (pdf) of X , $\Gamma(\alpha)$ is the Gamma function of parameter α ,

- (1) the domain of definition of $Ga(\alpha, \beta)$ is non-negative, and the shape shifting is mainly aroused by signal changing of parameters when Gaussian noise is utilized to sample the particles, so using noises in Gamma distribution makes sure that the signs of the parameters remains unchanged during iteration.
- (2) $E(X) = \alpha \cdot \beta^{-1}$, $var(X) = \alpha \cdot \beta^{-2}$, which makes it available to figure out the value of α, β by making the conversion from parameter values of Gaussian noise calculated by the algorithm easily.
- (3) when α and β draw relatively large values, Gamma distribution almost tends to be Gaussian distribution, so that the basic operation requirement of the UKF part in non-linear problems is satisfied to a large extent.

The shape shifting could be avoided by making use of Gamma distribution, but computational cost is ascending at the same time. As an alternative, resampling methods demands regularization repeatedly, or increased workload by more initial particles and longer iteration procedure using Gaussian noise with large variance to meet the supposed range.

So it is urgent to apply different scale of the distribution to sample within different stages, and the proposed state equations are as follows,

$$x_{i,k} = F \cdot x_{i,k-1} + cov(ukf(x_{i,k-1})) \cdot \rho_n, \quad i=1, 2, \dots, n \quad (12)$$

where ρ_n denotes the scale adjusting matrix, $cov(\cdot)$ denotes the covariance matrix determined by the calculation in the UKF part. Before the inflection point, ρ_n could be a diagonal matrix of constants like 1. As for the situation after the point, ρ_n could be a diagonal matrix to adjust the speed of iteration,

$$\rho_n = \begin{bmatrix} \rho_{e1k} & & & \\ & \rho_{e2k} & & \\ & & \rho_{e3k} & \\ & & & \rho_{e4k} \end{bmatrix} \quad (13)$$

where ρ_{e1k}, ρ_{e2k} are enormously larger than ρ_{e3k}, ρ_{e4k} in terms of the order of magnitudes indicating the changing of the dominant role of the part of measurement equation in the iteration after the inflection point, like $\rho_{e1k} = 1, \rho_{e2k} = 100, \rho_{e3k} = 0.1, \rho_{e4k} = 0.01$, which is used in the iteration of verifying the performance of the algorithm under 25°C 1C1C condition, and slightly adjusted to $\rho_{e1k} = 1, \rho_{e2k} = 50, \rho_{e3k} = 0.01, \rho_{e4k} = 0.01$ to make it suitable for RUL prediction under 35°C 1C1C condition.

Determined by the 95% confidence intervals of the fitting parameters, and considering the shape of the early term of the empirical model and the measurement noise, the inflection point is identified by a 3σ -interval criterion using filtered differential capacity curve.

It is noteworthy that, the inflection point is NOT the same as the true capacity diving point shown in Fig. 1. the inflection point determined by 3σ -interval criterion is the 478th, and the true capacity degradation point is found to be the 499th. This could be explained by that the inflection point is identified by training data, and the lower the capacity of the EOL point is set manually (usually 80% of initial capacity), the later the true capacity diving point is likely to appear. However in the cases discussed in this paper, the inflection point is found before the true capacity diving point, which makes it feasible to predict the capacity diving tendency using a little information after the inflection point *before* capacity diving appears. As an example, cyclic capacity degradation data up to 484 cycles under 45°C 1C1C condition are enough to train the proposed algorithm, with an accurate prediction result obtained.

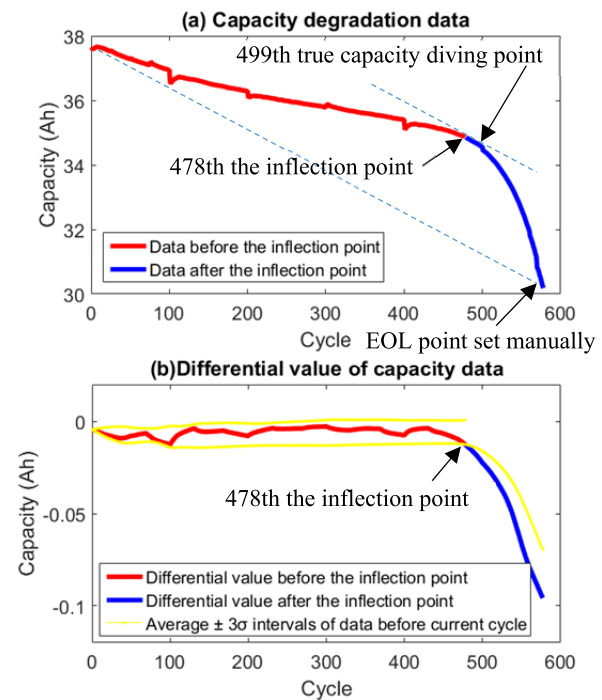


FIGURE 1. (a)Raw capacity data curve, and (b)Differential value of capacity degradation curve with 3σ -interval inflection point identification under the 45°C 1C1C condition.

More specifically, the inflection point reflects the changing of the dominant role of the part of measurement equation in the iteration, and the capacity diving point is defined as the most valuable point to determine in practice, the tangent line of which is parallel to the linkage of the initial point and the EOL point as in Fig. 1 for instance. In consequence, the inflection point in this study could imply a significant

beginning of another prediction, with the EOL point as the target of prediction.

III. RUL PREDICTION FRAMEWORK BASED ON IMPROVED UPF

The general UPF framework is introduced in [19], and the improved UPF steps effectively used in this paper is introduced with a flowchart in Fig. 2 and as follows,

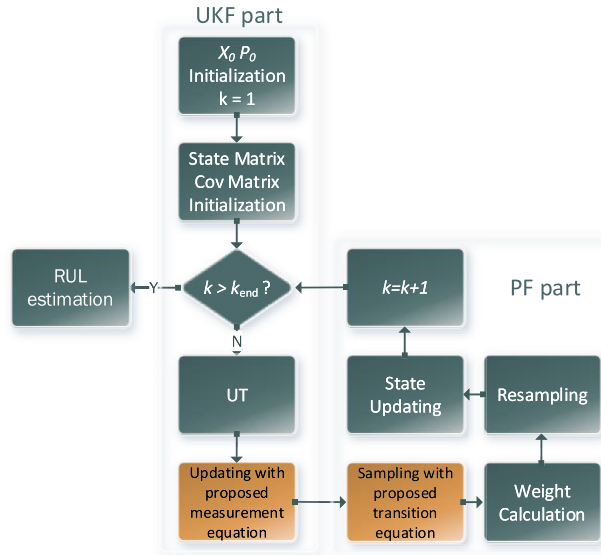


FIGURE 2. Flowchart of the improved UPF proposed in the paper with the improved parts colored in orange.

State space equations are established with (12) and (9) combined in (14),

$$\begin{cases} x_k = f(x_{k-1}, v_{k-1}) \\ z_k = h(x_k, n_k) \end{cases} \quad (14)$$

where x_k denotes the state of the system in moment k , z_k denotes the observed value, v_{k-1} denotes the systematic noise, and n_k denotes the measurement noise.

Step 1 (Initialization):

Generate $N_x = 200$ initial random particles $\{x_0\}_{i=1}^{N_x}$, where $x_0 = [a_0 \ b_0 \ c_0 \ d_0]^T$, $c_0 > 0$, $a_0, b_0, d_0 < 0$ as the fitting parameters of the training data up to the current point with the same weight $1/N_x$ for each particle.

$$\bar{x}_0 = E(x_0) \quad (15)$$

$$P_0 = E[(x_0 - \bar{x}_0)(x_0 - \bar{x}_0)^T] \quad (16)$$

Step 2 (State Matrix and Covariance Matrix):

$$x_0^a = [x_0^T \ 0 \ 0]^T \quad (17)$$

$$P_0^a = \begin{bmatrix} P_0 & 0 & 0 \\ 0 & Q_0 & 0 \\ 0 & 0 & R_0 \end{bmatrix} \quad (18)$$

Step 3 (Unscented Transformation):

$$x_k^a = [x_k^T \ v_k^T \ n_k^T]^T \quad (19)$$

$$P_k^a = \begin{bmatrix} P_k & 0 & 0 \\ 0 & Q_k & 0 \\ 0 & 0 & R_K \end{bmatrix} \quad (20)$$

$$x_k^a = [x_k^T \ v_k^T \ n_k^T]^T \quad (21)$$

$$x_{k-1}^x = [x_{k-1}^x \ x_{k-1}^v \ x_{k-1}^n]^T \quad (22)$$

where

$$\eta = \sqrt{n + \lambda} \quad (23)$$

$$\lambda = \alpha^2(n + k) - n, \quad (24)$$

$$x_{k-1}^a = [x_{k-1}^x \ x_{k-1}^v \ x_{k-1}^n]^T \quad (25)$$

$$W_0^{(m)} = \frac{\lambda}{n + \lambda} \quad (26)$$

$$W_0^{(c)} = \frac{\lambda}{n + \lambda} + 1 - \alpha^2 + \beta \quad (27)$$

$$W_i^{(m)} = W_i^{(c)} = \frac{\lambda}{2(n + \lambda)}, \quad i = 1, 2, \dots, 2n \quad (28)$$

where n denotes the quantity of the parameter dimension and W denotes the weights of the mean and covariance. It is assigned in the work that $\alpha = 1$, $\beta = 0$, $\lambda = 2$.

Step 4 (Parameters Update From Moment $k-1$ to k):

$$x_{k|k-1}^x = f(x_{k-1}^x, x_{k-1}^v) \quad (29)$$

$$\bar{x}_{k|k-1} = \sum_{i=0}^{2n} W_i^{(m)} x_{i,k|k-1}^k \quad (30)$$

$$P_{k|k-1} = \sum_{i=0}^{2n} W_i^{(c)} \left[x_{i,k|k-1}^k - \bar{x}_{k|k-1} \right] \times \left[x_{i,k|k-1}^k - \bar{x}_{k|k-1} \right]^T \quad (31)$$

$$Z_{k|k-1} = h(x_{k|k-1}^x, x_{k|k-1}^n) \quad (32)$$

$$\bar{Z}_{k|k-1} = \sum_{i=0}^{2n} W_i^{(c)} Z_{i,k|k-1} \quad (33)$$

$$P_{Z_{k|k-1} Z_{k|k-1}} = \sum_{i=0}^{2n} W_i^{(c)} \left[Z_{i,k|k-1} - \bar{Z}_{k|k-1} \right] \times \left[Z_{i,k|k-1} - \bar{Z}_{k|k-1} \right]^T \quad (34)$$

$$P_{x_{k|k-1} Z_{k|k-1}} = \sum_{i=0}^{2n} W_i^{(c)} \left[x_{i,k|k-1}^x - \bar{x}_{k|k-1} \right] \times \left[Z_{i,k|k-1} - \bar{Z}_{k|k-1} \right]^T \quad (35)$$

$$K_k = P_{Z_{k|k-1} Z_{k|k-1}} P_{x_{k|k-1} Z_{k|k-1}}^{-1} \quad (36)$$

where K_k is the filter gain used in the Kalman filter part,

$$\bar{x}_k = \bar{x}_{k|k-1} + K_k (Z_k - \bar{Z}_{k|k-1}) \quad (37)$$

$$\hat{P}_k = P_{k|k-1} - K_k P_{Z_{k|k-1} Z_{k|k-1}} K_k^T \quad (38)$$

Step 5 (Sampling):

$$\begin{aligned} \hat{x}_k^i &\sim q(x_k^i | x_{k-1}^i, z_k) \hat{P}_k = \hat{P}_k * \rho_n \\ &\Rightarrow \begin{cases} Ga(\bar{x}_k^2 \cdot \hat{P}_k^{i-1}, \bar{x}_k^i \cdot \hat{P}_k^{i-1}), & \bar{x}_k^i > 0 \\ -Ga(\bar{x}_k^2 \cdot \hat{P}_k^{i-1}, -\bar{x}_k^i \cdot \hat{P}_k^{i-1}), & \bar{x}_k^i < 0 \end{cases} \end{aligned} \quad (39)$$

As is illustrated in (12), ρ_n in the state transition equation works here to adjust the covariance matrix especially after the inflection point, adjusting the sampling value ranges to accelerate the speed of the correct convergence of iteration process.

On condition that α and β in $Ga(\alpha, \beta)$ are relatively large positive values, Gamma distribution almost tends towards Gaussian distribution. Nevertheless, the difference is that the domain of definition of $Ga(\alpha, \beta)$ is non-negative, which makes the signs of all the parameters unchanged with the sampled particles in a similar distribution to using Gaussian noise, where $E(X) = \alpha \cdot \beta^{-1} = \frac{\bar{x}_k^i \cdot \hat{P}_k^{i-1}}{\bar{x}_k^i \cdot \hat{P}_k^i} = \bar{x}_k^i$ and $var(X) = \alpha \cdot \beta^{-2} = \frac{\bar{x}_k^i \cdot \hat{P}_k^{i-1}}{(\bar{x}_k^i \cdot \hat{P}_k^{i-1})^2} = \hat{P}_k^i$. As a result of the conversion, the same tendency remains in the shape of the capacity degradation curve, and the basic operation requirement of the UKF part in non-linear problems is satisfied to a large extent, compared with the undesired likelihood that the prediction curve would be ascending later because of the changed sign of a certain parameter when the particles are sampled with Gaussian noise.

Step 6 (Weight Calculation)

$$\omega_k^i = \frac{p(x_{0:k}^i | z_{1:k})}{q(x_{0:k}^i | z_{1:k})} = \omega_{k-1}^i \frac{p(z_k | x_k^i) q(x_k^i | x_{k-1}^i)}{q(x_k^i | x_{k-1}^i, z_k)} \quad (40)$$

$$\omega_k^i = \frac{\omega_k^i}{\sum_{i=1}^N \omega_k^i} \quad (41)$$

where p denotes the pdf of the prior distribution, and q denotes the pdf of updated particles in Gamma distribution with parameters calculated by (39), and (40) is effective as long as $q(x_k^i | x_{k-1}^i, z_{1:k}) = q(x_k^i | x_{k-1}^i, z_k)$ is satisfied, with the recent measurement incorporated in the design of importance function by the proposed state space equations.

Step 7 (Multinomial Resampling):

$$\omega_k^i = \frac{1}{N} \quad (42)$$

This step is commonly used to resolve the particle degeneracy phenomenon. Resampling method introduced in [28] or any others effective could be an alternative here.

Step 8 (State Update):

$$\tilde{x}_k^i = \sum_{n=1}^N \omega_n^i x_n^i \quad (43)$$

$$P_k^i = \sum_{n=1}^N \omega_n^i [x_n^i - \tilde{x}_k^i] [x_n^i - \tilde{x}_k^i]^T \quad (44)$$

After $k = k + 1$, return to step 4 until the iteration moment k arrives at k_{end} .

Once the convergence speed of parameter value is slowed exceeding an experimental threshold, the last section of process will not have to continue anymore, thus k_{end} is attained earlier than standard UPF, which means less training information is necessary making further expansion of the advantages of UPF sampling in local iteration.

Step 9 (RUL Estimation):

RUL estimation value L_k^i of the i th particle using the training data up to the moment k can be solved by,

$$a_k^i \cdot e^{\frac{b_k^i}{(k+L_k^i)}} + c_k^i \cdot e^{d_k^i \cdot (k+L_k^i)} = C_{eol} \quad (45)$$

$$\bar{L}_k = \sum_{i=1}^N \omega_k^i L_k^i \quad (46)$$

The initial point $(0, H_0)$ and the EOL point (x_{EOL}, C_{eol}) are linked, to which the furthest point curve is determined as the true capacity diving point. The slope of the capacity diving point can be obtained by $(C_{eol} - H_0) \cdot x_{EOL}^{-1}$.

First order differential function of the measurement equation is shown in (47),

$$H'(x) = -\frac{abe^{\frac{b}{x}}}{x^2} + cde^{dx}, \quad x \in N^+, \quad c > 0, \quad a, b, d < 0 \quad (47)$$

and the capacity diving point x_d can be calculated by (48),

$$\begin{cases} \bar{a}_k \cdot e^{\bar{b}_k \cdot x_{EOL}^{-1}} + \bar{c}_k \cdot e^{\bar{d}_k \cdot x_{EOL}} = C_{eol} \\ -\frac{\bar{a}_k \bar{b}_k e^{\frac{\bar{b}_k}{x_d}}}{x_d^2} + \bar{c}_k \bar{d}_k e^{\bar{d}_k x_d} = (C_{eol} - H_0) \cdot x_{EOL}^{-1} \\ x_{EOL} = k + \bar{L}_k, \\ 0 < x_d < x_{EOL} \end{cases} \quad (48)$$

Actually, on condition that the EOL point is determined, the relevant prediction of both the capacity diving point and the RUL would be regarded as the same in degree of accuracy after calculating (45) and (48). So the prediction performance of the EOL point is representatively selected as the indicator in the following discussion to evaluate the proposed method in the paper.

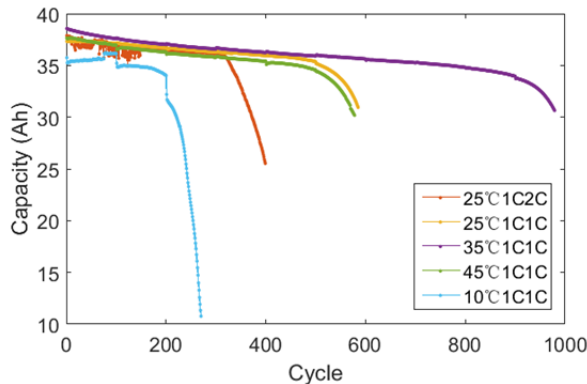
IV. EXPERIMENTAL VERIFICATIONS AND DISCUSSION

To verify the performance of all proposed methods, case studies are carried out where 15 pieces of Lithium-ion batteries with Li(NiMnCo)O₂ cathode (Rated capacity 36 Ah, Energy density 180 Wh/kg) are conducted cycle aging tests under different regular temperature conditions and regular current ratios. The observed capacity degradation data is shown in Fig. 3 with distinct capacity diving seen in the later part of each curve without exception, and the data points used to plot curves are generated from the mean value of each 3 batteries under the same working condition respectively.

A. VERIFICATION OF THE FITTING PERFORMANCE

Using statistical indicators in Table 2, comparisons are firstly made by least square fitting showing that under the majority of circumstances, the proposed model and the double exponential model are excellent to fit the curves with very little SSE and RMSE, as well as R² indicators extremely close to 1.

Besides, the proposed model attains better performance than the double exponential model in spite of almost the same under the 35°C1C1C condition, which is attributed to few data collected after the inflection point and very long flat early data curve. That is to say, the double exponential model is too smooth to describe a majority of the conditions with a relative sharp variation tendency. Moreover, the performance of 3-parameter empirical model indicates a really bad fitness to the situation.

**FIGURE 3.** Raw capacity degradation data.**TABLE 2.** Fitting performance of the models.

Data set	Model	SSE	RMSE	R^2	R_{adj}^2
10°C 1C1C 270 cycles	Proposed	46.8350	0.4196	0.9943	0.9942
	2exp	47.0966	0.4208	0.9943	0.9942
	Exp+polynomial	135.1153	0.7100	0.9835	0.9835
25°C 1C1C 585 cycles	Proposed	0.9959	0.0414	0.9988	0.9988
	2exp	1.3966	0.0490	0.9983	0.9983
	Exp+polynomial	69.9630	0.3467	0.9156	0.9153
25°C 1C2C 399 cycles	Proposed	35.0830	0.2980	0.9947	0.9946
	2exp	63.8962	0.4022	0.9903	0.9902
	Exp+polynomial	606.0797	1.2340	0.9078	0.9078
35°C 1C1C 979 cycles	Proposed	16.7597	0.1311	0.9914	0.9914
	2exp	14.4739	0.1218	0.9926	0.9925
	Exp+polynomial	112.6579	0.3397	0.9418	0.9417
45°C 1C1C 578 cycles	Proposed	6.4607	0.1061	0.9943	0.9942
	2exp	7.2494	0.1124	0.9936	0.9935
	Exp+polynomial	96.4925	0.4096	0.9143	0.9140

According to the capacity diving degradation shape and average value range of inflection point estimated, the sensitivity of the primary terms representing such a tendency of the curve is compared with an inflection point $x_i \sim 1e2$ empirically.

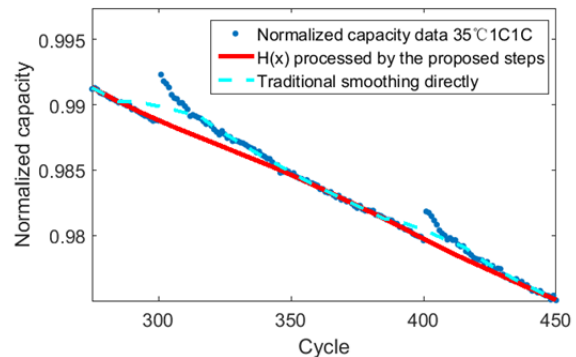
It is well acknowledged that sensitivity of a parameter illustrates the width of corresponding confidence intervals, hence the function term $ae^{\frac{b}{x}}$ owning small values in the critical neighborhood shown in Table 3 is preferably selected to the algorithm application for rapid convergence with the same amount of training information.

B. VERIFICATION OF THE PROPOSED PREPROCESSING METHOD

The case under the condition of normalized 37Ah 35°C 1C1C preprocessed is partly shown in Fig. 4. Fitting the curves using the proposed model in (9), the MSE considering the capacity recovery effect is reduced by more than 15.54% on the part of raw data, and reduced by approximately 13.81%

TABLE 3. Sensitivity of the parameters of the term representing the capacity diving.

Terms with ranges	$ 'a $	$ 'b $
$ae^{bx} _{b \sim +1e-2}^{a \sim -1e-10 \text{ to } -1e-11}$	$e^{bx} _{x=x_i} \text{ large to } x_i$	$axe^{bx} _{x=x_i} \text{ large}$
$ae^{\frac{b}{x}} _{b \sim -1e3 \text{ to } -1e4}^{a \sim -1e7 \text{ to } -1e8}$	$e^{\frac{b}{x}} _{x=x_i} \text{ small to } x_i$	$\frac{a}{x} \cdot e^{\frac{b}{x}} _{x=x_i} \text{ small}$
$ax^b _{b \sim +1e0}^{a \sim -1e-10}$	$x^b _{x=x_i} \text{ large to } x_i$	$a \ln x \cdot x^b _{x=x_i} \text{ large}$

**FIGURE 4.** Part of the preprocessed curve with and without the capacity self-recharge effect considered.

on the part of the curve preprocessed without considering the effect, of which the bias by direct smoothing in latter case is enormously intensified, attributed to the redundant unrelated information of the self-recharged capacity not involved in the empirical model $H(x)$.

C. VERIFICATION OF PREDICTION ACCURACY WITH CAPACITY DIVING

The 584th is calculated as the true EOL point, and the 581st as the actual final prediction of the 491st point with a percentage error of 0.513%, and an absolute error of 3 cycles shown in Fig. 6. It could also be concluded from iteration curve of parameter b in Fig. 5, that the prediction will show gradually fluctuation over the true value with reducing amplitude, making it unnecessary to train more subsequent points, thus ending the iteration.

To further illustrate the convergence tendency of the last several iterations, parameter c of the simplex exponential term in (9) representing the early stage amplitude, is given a value far from the true value shown in Fig. 7.

It can be concluded from iteration curve of parameter c in Fig. 7(b), that the parameter value c shows undoubtedly gradual fluctuation over the true value with reducing amplitude, which is a strong evidence proving the reasonability to end the iteration in the way described in the last section. And a similar prediction result of the EOL point is shown in Fig. 8, with little difference in particle distribution from Fig. 6.

However, the slowed degradation tendency to the true value of EOL point should not be regarded as the signal to end the iteration, for a very sharp decline appears in the later

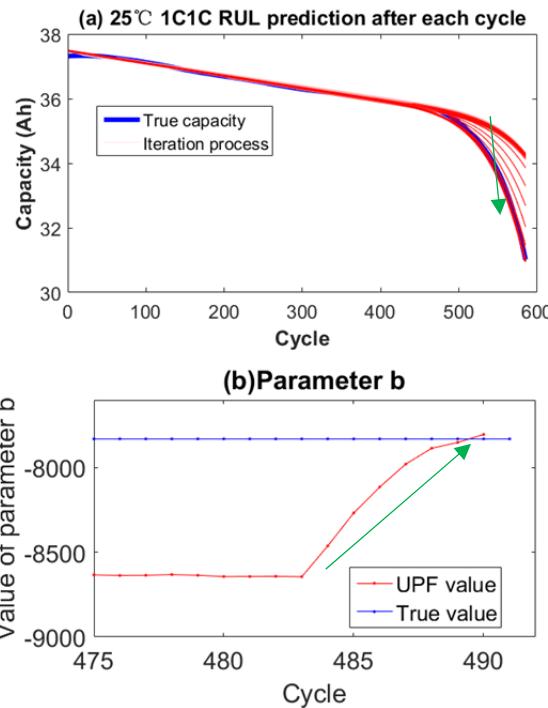


FIGURE 5. (a)Prediction curves starting at the corresponding moment during UPF iteration procedure, and (b)Parameter b value during latest UPF iteration procedure.

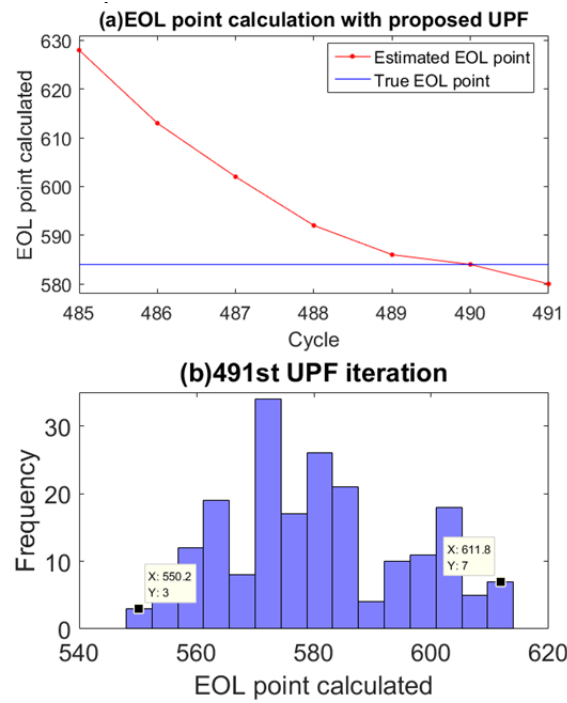


FIGURE 6. (a)The EOL point calculated by the proposed method, and (b) calculated EOL point distribution of particles after the 491st iteration.

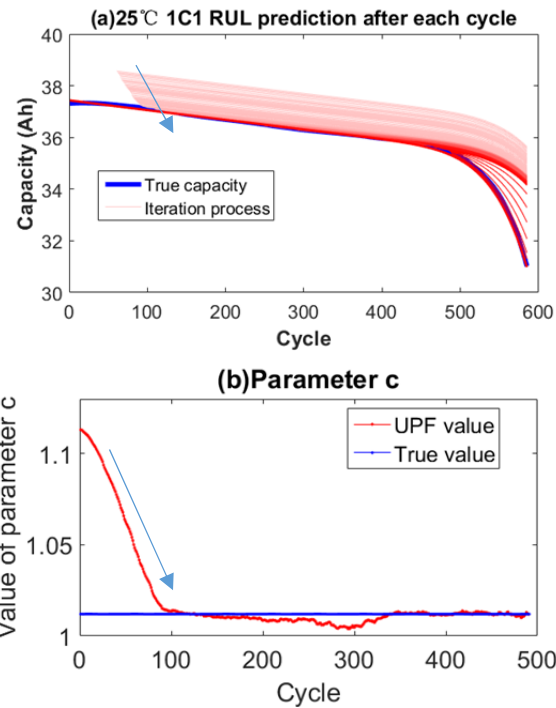


FIGURE 7. (a)Prediction curves starting at the corresponding moment during UPF iteration procedure, and (b)Parameter c value during UPF iteration procedure.

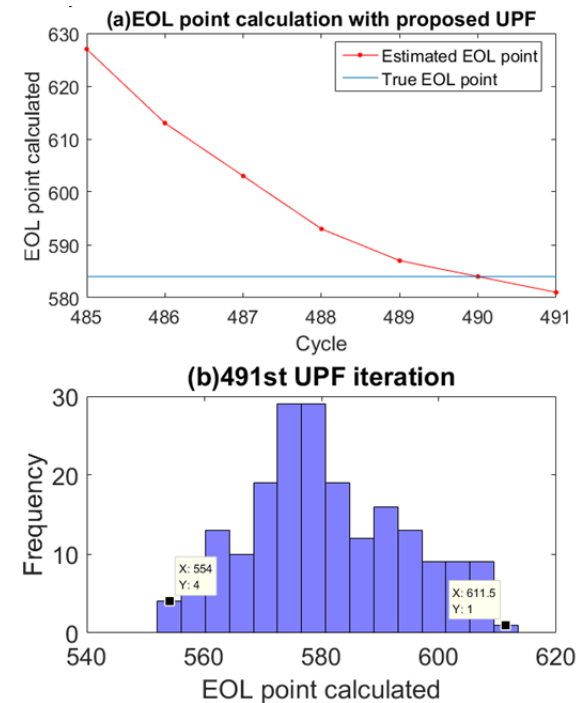


FIGURE 8. (a)The EOL point calculated by the proposed method with different initial parameters, and (b) Calculated EOL point distribution of particles after the 491st iteration with different initial parameters.

curve with capacity diving. Instead, it is well founded that the covariance matrix of the transition equation indicates the iteration procedure near the end by a gradual slowed variation

of the algorithm parameters. That is to say, even though some of the parameters reached the true value at certain moment, the EOL point calculated could have differed from the true

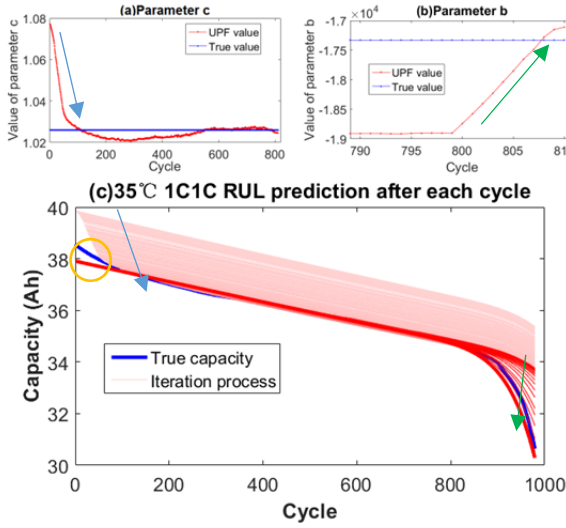


FIGURE 9. (a)Value of parameter c during UPF iteration procedure, (b)Value of parameter b during UPF iteration procedure, and (c)Predicted curves starting at the corresponding moment during the iteration procedure of UPF with initial parameters further to true fitting values of 35°C1C1C.

one, and vice versa. The same deduction can be drawn from the iteration curve of parameters to be verified in Fig. 9.

D. VERIFICATION OF PREDICTION ACCURACY WITH POOR INITIAL DATA QUALITY

The 809th is selected as the end of prediction point judged from Fig. 9(b), for an obvious gradual tendency approaching the true value with reducing amplitude can be seen in parameter b iteration curve, making it unnecessary to train more subsequent points. The 970th is calculated as the true EOL point, and the 965th as the predicted value of the 809th point with a percentage error of 0.515%, and an absolute error of 5 cycles shown in Fig. 10.

Though the activation effect of the batteries in the beginning cycles brings about several initial training data with poor quality, containing information not involved in the model within the orange circled part of the curve in Fig. 9, they have little influence on subsequent prediction, showing the excellent local iteration characteristics of UPF thanks to the quality-enhanced data by the proposed preprocessing method.

E. VERIFICATION OF FITTING PREDICTION ACCURACY IN EARLY CURVES

The proposed model shows satisfying performance in dealing with capacity diving degradation data sets, leading to another important qualitative comparison made to validate the performance when the models deal with the early part of the capacity degradation curve. In other words, if the capacity were not declining in a rapidly plunging way seen in the later curve, the performance should be figured out by fitting a relatively flat capacity degradation curve using the proposed

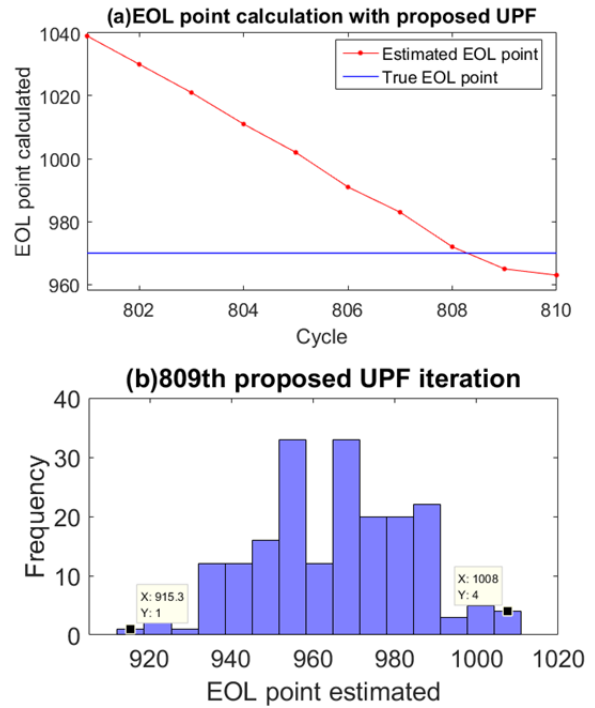


FIGURE 10. (a)The EOL point calculated by the proposed method, and (b) calculated EOL point distribution of particles after the 809th iteration.

TABLE 4. Least square fitting of 25°C1C1C data up to the inflection point.

Measurement equation	Fitting data used	Analytic expression of fittings
Proposed model	1/3(1~161 cycle)	$-5226 \cdot e^{-\frac{7237}{x}} + 37.42 \cdot e^{-8.812 \cdot 10^{-5}x}$
	1/2 (1~242 cycle)	$-8517 \cdot e^{-\frac{7487}{x}} + 37.45 \cdot e^{-9.955 \cdot 10^{-5}x}$
2-exp model	1/3 (1~161 cycle)	$37.54 \cdot e^{-3.613 \cdot 10^{-8}x} - 0.1736 \cdot e^{0.008737x}$
	1/2 (1~242 cycle)	$38.31 \cdot e^{-1.595 \cdot 10^{-8}x} - 0.9110 \cdot e^{0.002832x}$

model,

$$H(x) = ae^{\frac{b}{x}} + ce^{dx} + v_x, \quad x \in N^+, \quad c > 0, \quad a, b, d < 0 \quad (49)$$

and the double-exponential model with restricted value ranges,

$$H(x) = a_1 e^{b_1 x} + a_2 e^{b_2 x} + v_x, \quad x \in N^+, \quad a_1, b_1 > 0, \quad a_2, b_2 < 0 \quad (50)$$

The restricted value ranges bring the feasibility to make comparisons, because in order to ensure the stability of the algorithm, model parameters should not change their signs during iteration, which prevents the shape of the model shifting in obscure after the assumed inflection point.

Respectively, verification is made using 1/3 of the total unaccelerated degradation data as the training data, up to

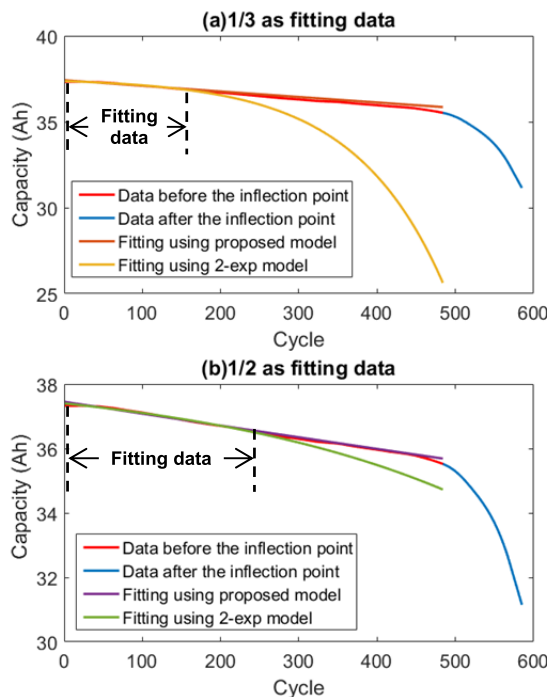


FIGURE 11. Least square fitting results of 25°C C1C1C data up to the inflection point (a) 1/3 as fitting data (b) 1/2 as fitting data.

TABLE 5. Performance of different model and methods.

Items of the EOL prediction	Proposed model and improved UPF		Conventional double exponential model and PF based methods	
	25°C 1C1C	35°C 1C1C	25°C C1C1C	35°C C1C1C
Absolute error (cycles)	3	5	11	19
Percentage error (%)	0.514	0.515	1.91	1.96
Particle pdf width (cycles)	61.6 57.5	92.7	>100	>100

161st, and 1/2 up to 242nd in Fig. 11. It is evident that fitting result of the two kinds of feasible capacity diving degradation models, with a number of early data shows different subsequent accuracy. More training information leads to better early part fitting performance of both equations, but the proposed shape in (48) is qualitatively much better fitted than the double exponential shape in (50).

F. PERFORMANCE OF DIFFERENT MODEL AND METHODS

Fitting performance comparison of the whole data between measurement models has been implemented in Table 2, and using the same training data under two conditions, prediction performance of the proposed model using improved UPF is compared with the conventional double exponential model with particle filter based methods in Table 5, where reduced error of estimation and narrowed width of confidence intervals by the proposed method can be obtained, implying the expected improvements achieved.

V. CONCLUSION

A systematic RUL prognostic method has been proposed in this paper, for Lithium-ion batteries with Li(NiMnCo)O₂ cathode with distinct capacity diving in later lifetime cycles using improved UPF.

- (1) In pursuit of further accuracy of the model, the quality of the training data is enhanced by taking the capacity recovery phenomenon into account, as well as using Savitzky-Golay filtering. With the training data such preprocessed after outlier elimination, a decrease in the fitting RSE of training data can be attained.
- (2) In order to use the empirical model in RUL prediction, an appropriate measurement equation is proposed under the consideration of capacity diving in later capacity degradation curve. Validation result indicates that the fitting performance and parameter sensitivity could be found more excellent statistically when the proposed model is applied to almost all of the cases compared with others including popular double-exp.
- (3) An improved state transition model has been utilized in UPF iteration containing the sectioned treatment technique of sampling by using inflection point checking and systematic noise in Gamma distribution. To find out when to end the iteration, prediction curves during UPF iterations have been drawn with the accelerated convergence tendency implied clearly, and potential shape shifting of the prediction curve is prevented, thus robustness of the method guaranteed.
- (4) An overall flowchart of the proposed systematic framework contained is developed with the steps summarized. Due to the improved state space equations, it has been achieved that using the same amount of training information, enhanced accuracy of the prediction could be obtained in predicting EOL point effectively, which is also true of the fitting prediction before the inflection point.

Owing to the restrictions of training data acquisition, the source of the training information discussed in this paper is limited to the cyclic capacity data only. As a supplement to the space state equations, incremental capacity analysis (ICA) of cyclic capacity-voltage data and other methods will be very helpful to the verification of capacity diving in our future work, which could also be extended by improving the analytical form of the empirical capacity degradation model or combining the proposed UPF with data-driven methods to reduce the error.

REFERENCES

- [1] W. Waag, C. Fleischer, and D. U. Sauer, "Critical review of the methods for monitoring of lithium-ion batteries in electric and hybrid vehicles," *J. Power Sources*, vol. 258, pp. 321–339, Jul. 2014.
- [2] A. Barré, B. Deguilhem, S. Grolleau, M. Gérard, F. Suard, and D. Riu, "A review on lithium-ion battery ageing mechanisms and estimations for automotive applications," *J. Power Sources*, vol. 241, pp. 680–689, Nov. 2013.

- [3] S. Tippmann, D. Walper, L. Balboa, B. Spier, and W. G. Bessler, "Low-temperature charging of lithium-ion cells part I: Electrochemical modeling and experimental investigation of degradation behavior," *J. Power Sources*, vol. 252, pp. 305–316, Apr. 2014.
- [4] A. Cordoba-Arenas, S. Onori, Y. Guezennec, and G. Rizzoni, "Capacity and power fade cycle-life model for plug-in hybrid electric vehicle lithium-ion battery cells containing blended spinel and layered-oxide positive electrodes," *J. Power Sources*, vol. 278, pp. 473–483, Mar. 2015.
- [5] W. He, N. Williard, M. Osterman, and M. Pecht, "Prognostics of lithium-ion batteries based on Dempster-Shafer theory and the Bayesian Monte Carlo method," *J. Power Sources*, vol. 196, no. 23, pp. 10314–10321, Dec. 2011.
- [6] W. Gu, Z. Sun, X. Wei, and H. Dai, "A capacity fading model of lithium-ion battery cycle life based on the kinetics of side reactions for electric vehicle applications," *Electrochim. Acta*, vol. 133, pp. 107–116, Jul. 2014.
- [7] Y. Zhang, R. Xiong, H. He, and M. G. Pecht, "Long short-term memory recurrent neural network for remaining useful life prediction of lithium-ion batteries," *IEEE Trans. Veh. Technol.*, vol. 67, no. 7, pp. 5695–5705, Jul. 2018.
- [8] D. Wang, Q. Miao, and M. Pecht, "Prognostics of lithium-ion batteries based on relevance vectors and a conditional three-parameter capacity degradation model," *J. Power Sources*, vol. 239, pp. 253–264, Oct. 2013.
- [9] D. Liu, J. Zhou, D. Pan, Y. Peng, and X. Peng, "Lithium-ion battery remaining useful life estimation with an optimized relevance vector machine algorithm with incremental learning," *Measurement*, vol. 63, pp. 143–151, Mar. 2015.
- [10] Y. Zhou and M. Huang, "Lithium-ion batteries remaining useful life prediction based on a mixture of empirical mode decomposition and ARIMA model," *Microelectron. Rel.*, vol. 65, pp. 265–273, Oct. 2016.
- [11] M. Ibrahim, N. Steiner, S. Jemei, and D. Hissel, "Wavelets-based approach for online fuel cells remaining useful lifetime prediction," *IEEE Trans. Ind. Electron.*, vol. 63, no. 8, pp. 5057–5068, Aug. 2016.
- [12] B. Saha, K. Goebel, and J. Christoffersen, "Comparison of prognostic algorithms for estimating remaining useful life of batteries," *Trans. Inst. Meas. Control*, vol. 31, nos. 3–4, pp. 293–308, Jun./Aug. 2009.
- [13] W. Xian, B. Long, M. Li, and H. Wang, "Prognostics of lithium-ion batteries based on the verhulst model, particle swarm optimization and particle filter," *IEEE Trans. Instrum. Meas.*, vol. 63, no. 1, pp. 2–17, Jan. 2014.
- [14] D. Zhou, A. Al-Durra, K. Zhang, A. Ravey, and F. Gao, "A robust prognostic indicator for renewable energy technologies: A novel error correction grey prediction model," *IEEE Trans. Ind. Electron.*, vol. 66, no. 12, pp. 9312–9325, Dec. 2019.
- [15] X.-S. Si, "An adaptive prognostic approach via nonlinear degradation modeling: Application to battery data," *IEEE Trans. Ind. Electron.*, vol. 62, no. 8, pp. 5082–5096, Aug. 2015.
- [16] S. Tang, C. Yu, X. Wang, X. Guo, and X. Si, "Remaining useful life prediction of lithium-ion batteries based on the Wiener process with measurement error," *Energies*, vol. 7, no. 2, pp. 520–547, Jan. 2014.
- [17] Z.-X. Zhang, X.-S. Si, C.-H. Hu, and M. G. Pecht, "A prognostic model for stochastic degrading systems with state recovery: Application to li-ion batteries," *IEEE Trans. Rel.*, vol. 66, no. 4, pp. 1293–1308, Dec. 2017.
- [18] M. Vemula, M. F. Bugallo, and P. M. Djuric, "Performance comparison of Gaussian-based filters using information measures," *IEEE Signal Process. Lett.*, vol. 14, no. 12, pp. 1020–1023, Dec. 2007.
- [19] Q. Miao, L. Xie, H. Cui, W. Liang, and M. Pecht, "Remaining useful life prediction of lithium-ion battery with unscented particle filter technique," *Microelectron. Rel.*, vol. 53, no. 6, pp. 805–810, Jun. 2013.
- [20] K. A. Severson, P. M. Attia, N. Jin, N. Perkins, B. Jiang, Z. Yang, M. H. Chen, M. Aykol, P. K. Herring, D. Fragedakis, M. Z. Bazant, S. J. Harris, W. C. Chueh, and R. D. Braatz, "Data-driven prediction of battery cycle life before capacity degradation," *Nature Energy*, vol. 4, no. 5, pp. 383–391, Mar. 2019.
- [21] H. Chen, P. Pei, and M. Song, "Lifetime prediction and the economic lifetime of proton exchange membrane fuel cells," *Appl. Energy*, vol. 142, pp. 154–163, Mar. 2015.
- [22] B. Mo, J. Yu, D. Tang, H. Liu, and J. Yu, "A remaining useful life prediction approach for lithium-ion batteries using Kalman filter and an improved particle filter," in *Proc. IEEE Int. Conf. Prognostics Health Manage. (ICPHM)*, Jun. 2016, pp. 1–5.
- [23] S. Zhang, "A new method for lithium-ion battery's SOH estimation and RUL prediction," in *Proc. 13th IEEE Conf. Ind. Electron. Appl. (ICIEA)*, May 2018, pp. 2693–2697.
- [24] L. Ungurean, G. Cârstoiu, M. V. Micea, and V. Groza, "Battery state of health estimation: A structured review of models, methods and commercial devices," *Int. J. Energy Res.*, vol. 41, no. 2, pp. 151–181, Jul. 2016.
- [25] X. Pang, R. Huang, J. Wen, Y. Shi, J. Jia, and J. Zeng, "A lithium-ion battery RUL prediction method considering the capacity regeneration phenomenon," *Energies*, vol. 12, no. 12, p. 2247, Jun. 2019.
- [26] L. Zhao, Y. Wang, and J. Cheng, "A hybrid method for remaining useful life estimation of lithium-ion battery with regeneration phenomena," *Appl. Sci.*, vol. 9, no. 9, p. 1890, May 2019.
- [27] R. R. Richardson, C. R. Birk, M. A. Osborne, and D. A. Howey, "Gaussian process regression for *in situ* capacity estimation of lithium-ion batteries," *IEEE Trans. Ind. Informat.*, vol. 15, no. 1, pp. 127–138, Jan. 2019.
- [28] H. Zhang, Q. Miao, X. Zhang, and Z. Liu, "An improved unscented particle filter approach for lithium-ion battery remaining useful life prediction," *Microelectron. Rel.*, vol. 81, pp. 288–298, Feb. 2018.
- [29] L. Li, A. A. F. Saldivar, Y. Bai, and Y. Li, "Battery remaining useful life prediction with inheritance particle filtering," *Energies*, vol. 12, no. 14, p. 2784, Jul. 2019.
- [30] X. Xu, C. Yu, S. Tang, X. Sun, X. Si, and L. Wu, "Remaining useful life prediction of lithium-ion batteries based on Wiener processes with considering the relaxation effect," *Energies*, vol. 12, no. 9, p. 1685, May 2019.
- [31] D. Wang, F. Yang, K.-L. Tsui, Q. Zhou, and S. J. Bae, "Remaining useful life prediction of lithium-ion batteries based on spherical cubature particle filter," *IEEE Trans. Instrum. Meas.*, vol. 65, no. 6, pp. 1282–1291, Jun. 2016.



XINWEI CONG (Student Member, IEEE) was born in Shandong, China. He received the bachelor's degree in electrical engineering from Beijing Jiaotong University, Beijing, China, in 2015, where he is currently pursuing the Ph.D. degree.

He is currently with the National Active Distribution Network Technology Research Center, Beijing Jiaotong University. His research interests include flexible connections of batteries, battery capacity prediction, and safety on battery packs.



CAIPING ZHANG (Senior Member, IEEE) was born in Henan, China. She received the B.S. degree in vehicular engineering from the Henan University of Science and Technology, Luoyang, China, in 2004, and the Ph.D. degree in vehicle engineering from the Beijing Institute of Technology, Beijing, China, in 2010.

She is currently a Professor with Beijing Jiaotong University, Beijing. Her research interests include battery modeling, state estimation, optimal charging, battery second use technology, and battery energy-storage systems.



JIUCHUN JIANG (Senior Member, IEEE) was born in Jilin, China. He received the B.S. degree in electrical engineering and the Ph.D. degree in power system automation from Northern Jiaotong University, Beijing, China, in 1993 and 1999, respectively.

He was a Professor with the School of Electrical Engineering, Beijing Jiaotong University, Beijing, until 2018. He is currently with the Hubei University of Technology, Hubei. His research interests include battery application technology, electric car charging stations, and microgrid technology. He was a recipient of the National Science and Technology Progress Second Award for his work on electric vehicle (EV) bus systems and the Beijing Science and Technology Progress Second Award for his work on EV charging systems.



WEIGE ZHANG was born in Gansu, China. He received the M.S. and Ph.D. degrees in electrical engineering from Northern Jiaotong University, Beijing, China, in 1997 and 2013, respectively. From 1993 to 1994, he was an Engineer with Hohhot Railway Bureau. He is currently a Professor with the School of Electrical Engineering, Beijing Jiaotong University, Beijing. His research interests include battery pack application technology, power electronics, and intelligent distribution systems.



XINYU JIA was born in Guangxi, China. He received the M.S. degree in electrical engineering from Beijing Jiaotong University, Beijing, China, in 2019, where he is currently pursuing the Ph.D. degree.

He is currently with the National Active Distribution Network Technology Research Center, Beijing Jiaotong University. His research interests include battery modeling and safety on batteries.



YAN JIANG was born in Jilin, China. He received the B.S. and Ph.D. degrees in electrical engineering from Beijing Jiaotong University, Beijing, China, in 2014 and 2020, respectively. From 2018 to 2019, he conducted scientific research as a joint Ph.D. Student at the DOE GATE Center for Electric Drive Transportation and the Department of Electrical and Computer Engineering, San Diego State University, San Diego, CA, USA. He is currently with Sunwoda Electronic Company Ltd., Shenzhen, China. He is also a Postdoctoral Researcher with the South China University of Technology, Guangzhou, China. His research interests include battery state estimation, battery second use technology, and battery energy storage systems.